MODELLING THE RELATIONSHIP BETWEEN LIQUID WATER CONTENT AND CLOUD DROPLET NUMBER CONCENTRATION OBSERVED IN SOME LOW CLOUDS IN THE SUMMER ARCTIC AND ITS RADIATIVE EFFECTS

by

Joelle Dionne

Submitted in partial fulfilment of the requirements
for the degree of Master of Science

at

Dalhousie University
Halifax, Nova Scotia
August 2018

DEDICATION PAGE

To my parents, for their unrelenting support, and to my friends, for my continued mental health.

TABLE OF CONTENTS

LIST OF TABLES

LIST OF FIGURES

ABSTRACT

We investigated the microphysical properties of some low Arctic clouds and attempted to simulate the observed linear relationship between liquid water content and cloud droplet number concentration. The low clouds were observed by an aircraft campaign based out of Resolute Bay conducted as a part of NETCARE in July 2014. We attempted to simulate this relationship using the Single Column Model for Arctic Boundary Layer Clouds (SCM-ABLC), and compared the radiative effect of the modelled and observed clouds using a single-column version of the radiative transfer model used in version 18 of the Canadian Atmospheric Model (CanAM4.3). The relationship was reasonably represented by the SCM-ABLC, and all three autoconversion parameterizations tested agreed with the radiative transfer calculated from observations.

LIST OF ABBREVIATIONS AND SYMBOLS USED

AIMMS	Aircraft Integrated Meteorological Measurement System
CanAM4	Canadian Atmospheric Global Climate Model, version 4
CanAM4.3	Canadian Atmospheric Global Climate Model, version 4.3
CCCma	Canadian Centre for Climate Modelling and Analysis
CCN	Cloud Condensation Nuclei
CDNC	Cloud Droplet Number Concentration
ECMWF	European Centre for Medium-Range Weather Forecasts
ERA	ECMWF Re-Analysis
ESDIS	Earth Science Data and Information System
FSSP	Forward Scattering Spectrometer Probe
LWC	Liquid Water Content
LWP	Liquid Water Path
m	metre
NASA	National Aeronautics and Space Administration
NETCARE	Network on Climate and Aerosols: Addressing Key Uncertainties in Remote Canadian Environments
SCM	Single Column Model
SCM-ABLC	Single Column Model for Arctic Boundary Layer Clouds
μm	10^{-6} metres

ACKNOWLEDGEMENTS

I would like to acknowledge the support of my supervisors, Dr. Rachel Chang and Dr. Ian Folkins, and my committee members, Dr. Randall Martin and Dr. Glen Lesins.

We acknowledge the use of imagery from the NASA Worldview application (https://worldview.earthdata.nasa.gov/) operated by the NASA/Goddard Space Flight Center Earth Science Data and Information System (ESDIS) project.

CHAPTER 1 INTRODUCTION

1.1. Radiative Effects of Clouds

Climate modelling and observations have shown that the Arctic is very sensitive to climate change (ACIA, 2005). One known uncertainty in our understanding of climate change is the effect of clouds on the radiation budget. There are feedbacks in the radiative budget due to cloud liquid water content (LWC), effective radius, and cloud droplet number concentration (CDNC). For instance, in the Arctic, smaller droplets are associated with less shortwave and more longwave radiation at the surface than larger droplets due to the increased reflectivity (shortwave radiation coming from the sun and longwave from the ground means more of each is reflected backwards toward its origin), but the net radiative effect of cloud droplet sizes is unclear (Curry et al., 1996). Overall, the radiative forcing from shortwave radiation due to cloud is dominated by the effects of cloud microphysics (including LWC, CDNC, and effective radius), solar zenith angle, and albedo (Curry et al., 1996). Similarly, the longwave cloud radiative forcing is dominated by the LWC, effective radius, phase of the cloud droplets, and emission temperature of the cloud (Sedlar et al., 2010). The droplet size distribution was found to have a small impact on radiation and LWC in a fog case study conducted in the mid-latitudes (Zhang et al., 2014), but it is unknown if this extends to clouds in the Arctic.

Results from a study of Arctic stratus clouds suggest that shortwave radiation has a large impact on the evolution of the clouds, as model runs without shortwave radiation had increased cloud depths and LWC, as well as larger cloud-top radiative cooling rates and

cooling through more of the cloud (Olsson et al., 1998). That study also found that the partitioning of radiant energy in the cloud is likely determined by droplet distributions, but the heating rate of the cloud constrains the circulation in the cloud and hence the microphysics (Olsson et al., 1998). As such, the relationship between cloud microphysics (e.g. droplet size distribution, total concentration, liquid water content) and cloud radiative balance may involve positive feedbacks. It is clear that the microphysics and radiative balance of the cloud are closely linked.

Studies have also evaluated the relative strengths and weaknesses of various schemes used in cloud modelling that affect radiative properties. As the summer Arctic surface is usually fairly clean of pollution transported from lower latitudes, the observational study FIRE.ACE suggested that the cloud albedo should be negatively correlated with cloud droplet effective radius during this time (Peng et al., 2002); it also showed that the cloud albedo increased with CDNC (Peng et al., 2002). However, a limitation of this study was that their results assumed homogeneous clouds on a global climate model-sized grid scale (often greater than 1 degree by 1 degree), with no possibility of adjustment for non-uniform CDNC or LWC (Peng et al., 2002). Comparing several models has supported the hypothesis that under very clean conditions, clouds can be very sensitive to cloud condensation nuclei (CCN) concentrations, to the point that the LWC and radiative effects of the clouds are CCN-limited (Stevens et al., in review). This comparison further suggested that models using faster autoconversion rates per unit cloud droplet mass are generally less sensitive to changes in CDNC or CCN concentrations for all of the cloud properties that were examined (Stevens et al., in review). However, the examined models

were different, and did not allow for the direct comparison of different autoconversion parameterizations using the same model. Furthermore, that study did not take into account the sensitivity of Arctic clouds to CCN concentrations or the rain formation in the model (Stevens et al., in review).

1.2. Observations from the NETCARE 2014 Flight Campaign

The observations that prompted our current case study were taken from the July 2014 flight campaign based in Resolute Bay, Nunavut, which was conducted by the Network on Climate and Aerosols: Addressing Key Uncertainties in Remote Canadian Environments (NETCARE). This study primarily relies on observations from the Forward Scattering Spectrometer Probe, the FSSP-100, which was used to measure the number and size of cloud droplets. The FSSP uses a laser beam to count the droplets and uses the scatter to determine the size of the droplets (Coelho et al., 2005).

Based on these measurements, a strong linear dependence between LWC and CDNC was found in low altitude clouds (Leaitch et al., 2016). In contrast, very little correlation was observed between LWC and CDNC in high altitude clouds (Leaitch et al., 2016). The low-level clouds showed no correlation between the LWC and the volume mean diameter (which was roughly constant), which may have indicated a lack of entrainment and clouds that do not show droplet growth with lifting (Leaitch et al., 2016). The 2014 NETCARE flight campaign was “the first collection of simultaneous observations of the microphysics of aerosols and clouds in this unique regime in which the net radiative impact of increases in the CDNC is hypothesized to be warming due to changes in the

LWC" (Leaitch et al., 2016). One goal of this project was to recreate the linear relationship that was observed between the LWC and CDNC in the low altitude clouds by Leaitch et al. (2016) using the Single Column Model for Arctic Boundary Layer Clouds (SCM-ABLC).

It is interesting to note that many of the low cloud cases observed during the NETCARE 2014 flight campaign had cloud droplet number concentrations at or below the Mauritsen limit (Leaitch et al., 2016). This limit is also described as the tenuous cloud regime; it occurs when cloud formation is limited by available CCN (Mauritsen et al., 2011). Further, cloud LWC is limited as droplets or CCN are necessary for condensation and deposition to occur; cloud LWC is also limited as the small number of droplets promotes faster growth and hence fallout (Mauritsen et al., 2011). This study explores whether there is a perceptible effect from the Mauritsen limit on the modelled relationship between LWC and CDNC as three of the eleven profiles that we examined had mean CDNC around or below the Mauritsen limit of 16/cm^3, as determined by Leaitch et al. (2016).

1.3. Single Column Models

In order to recreate the observed relationship between LWC and CDNC via modelling, we used a single column model (SCM). An SCM is a meteorological model that has no horizontal extent, only vertical. As such, it requires less computational time than a three-dimensional model that has the same vertical resolution. This can be an advantage when dealing with clouds, which often require fine vertical resolution for forecasting or other

modelling accuracy. Previous studies using SCMs have found that their suitability depends strongly on location and meteorological situation. Many meteorological phenomena that are predominantly driven by local influences can be better modelled by SCMs than by numerical weather prediction (NWP) models, as they are better modelled as a single horizontal point with many vertical layers than as something smaller than the size of the horizontal grid box in a three-dimensional model (Gultepe, 2007). Single column models can also assimilate observations that do not necessarily have wide spatial representation, and parameterization schemes are more easily adapted for one dimension (Terradellas and Cano, 2007).

Many of the disadvantages of SCMs can be accounted for. For example, SCMs cannot estimate any variables that depend on horizontal extent or use these variables in other calculations. As such, they must be assumed to be small in comparison to the other model processes, which only occurs over flat areas and when the local meteorology is relatively horizontally homogeneous (Terradellas and Cano, 2007). However, some small local adaptations can be made using additional forcings introduced into the model to make up for these missing variables. These forcings can be calculated from the local climatology, the output from three-dimensional models, or by running the model multiple times with different attempted forcings to find the best results (Terradellas and Cano, 2007). However, this introduces additional assumptions and can cause other problems in the model (Gultepe 2007). In our study, we addressed the missing model processes and local effects by using Newtonian relaxation techniques, which are further discussed in section 2.2.4.

1.3.1. Autoconversion Schemes

Autoconversion schemes use parameterizations to convert cloud droplets to drizzle drops in order to simulate rain. They are used instead of an explicit calculation of the cloud droplet size distribution in order to lower the computational cost and complexity of the model. The explicit calculation of the droplet size distribution would require all drops to be put into size bins, which would then have advection, condensation, coalescence, and other such processes enacted upon them, separately and at large computational cost. In comparison, autoconversion schemes depend on the prescribed shape of the droplet size distribution. These are often gamma or lognormal distributions (Khairoutdinov and Kogan, 2000).

It is more common, from cloud- to global-scale models, that several moments (e.g. liquid water content, cloud droplet number concentration, effective radius) of the droplet size distribution are predicted rather than the actual distribution; these moments are called bulk microphysics or bulk parameters (Khairoutdinov and Kogan, 2000). When explicit calculations are carried out, there is no need for an autoconversion scheme since the conversion of cloud water to rain drops is included in the calculation. Autoconversion schemes are needed when only the shape of the droplet size distribution is prescribed, since the rate of mass transfer from water vapour to cloud droplets depends not only on the bulk microphysics, but also on other properties of the droplet size distribution, which need to be parameterized (Khairoutdinov and Kogan, 2000). One method of parameterization is to relate autoconversion and accretion to the bulk parameters (Wood,

2005); this is done in the Khairoutdinov and Kogan (2000) scheme. Another method is to assume the form of the droplet size distribution and then relate the autoconversion and accretion to bulk parameters by simplifying the analytical forms (Wood, 2005); this is done in the Liu and Daum (2004) scheme. Autoconversion rates from different parameterizations can vary by up to three orders of magnitude for marine boundary layer clouds (Wood, 2005), so the choice of autoconversion scheme appears to be significant. Three autoconversion parameterizations from the literature were examined in this study: Khairoutdinov and Kogan (2000), Liu and Daum (2004), and Wood (2005). They are further discussed in section 2.2.5.

1.4. Summary

There is still work to be done on the topic of modelling clouds and their radiative effects in the summer Arctic. The autoconversion schemes described above have not been examined in the context of summer Arctic clouds. The linear relationship between cloud LWC and CDNC in the Arctic has been observed, but has not yet been reproduced by a model, so it is unknown if the current models can reproduce the relationship between these bulk parameters. The sensitivity of the radiative balance of the cloud to this relationship also does not appear to have been previously examined in detail or with respect to the autoconversion schemes we are interested in. To this end, this study examines the effects of different autoconversion schemes on the relationship between LWC and CDNC with a single-column model. We also examine if the differences between the various linear relationships of CDNC and LWC resulting from the different autoconversion schemes significantly change the radiative balance of the cloud. The

goals of this study are to reproduce the relationship between LWC and CDNC and to examine the sensitivity of the radiative impacts of this relationship to the autoconversion schemes used to model it. This is accomplished by using the SCM-ABLC and investigating the results of its three autoconversion schemes with version 18 of the Canadian Centre for Climate Modelling and Analysis (CCCma) Radiative Transfer Model.

CHAPTER 2 METHODS

2.1. Observations

2.1.1 Overview

In order to simulate the observed LWC to CDNC relationship from observed clouds and to examine their radiative effects, we used observations from the Network on Climate and Aerosols: Addressing Key Uncertainties in Remote Canadian Environments (NETCARE) project. These data were collected during an aircraft campaign based out of Resolute Bay, Nunavut, in July 2014. Full details of the flight campaign are described by Leaitch et al. (2016).

2.1.2 Description of Observations

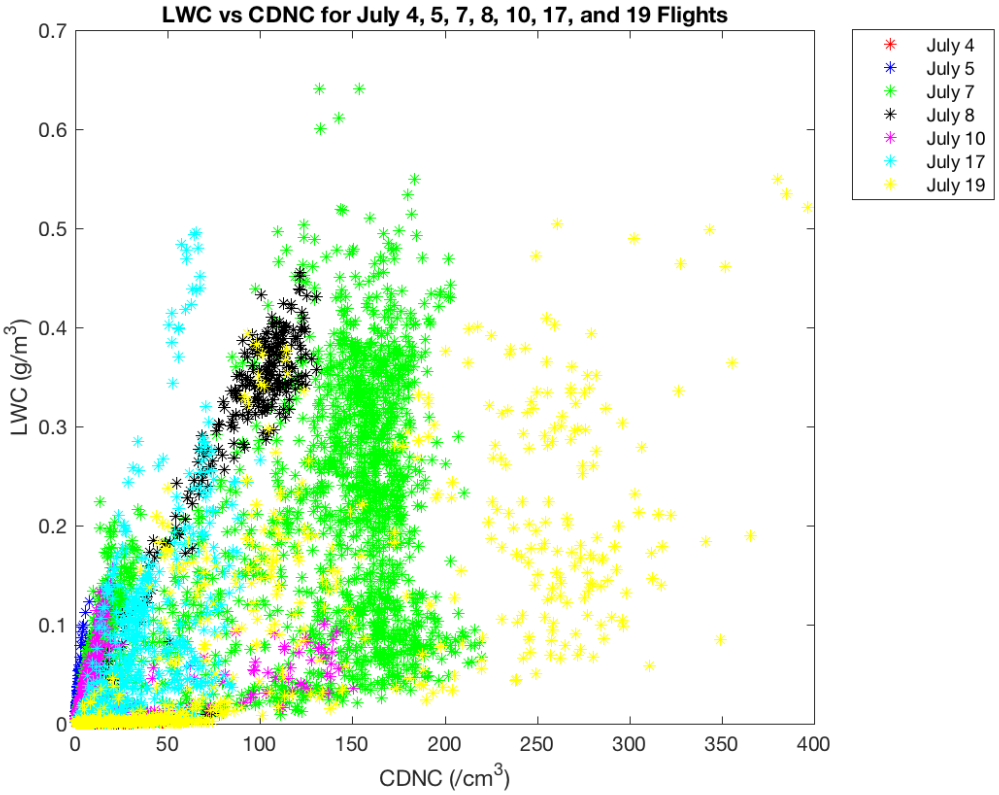

Figure 2.1. The relationships between LWC and CDNC during all times and at all altitudes and locations during the NETCARE 2014 flight campaign. There is no linear relationship between all of these data.

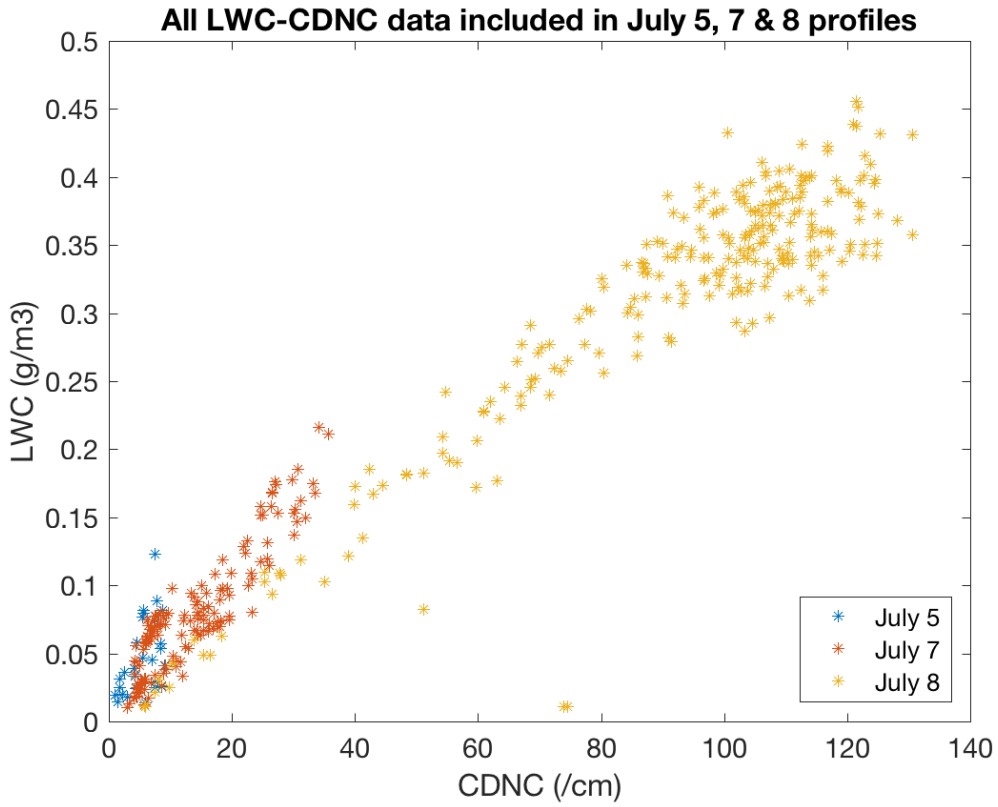

Figure 2.2. The observed linear relationship between LWC and CDNC at every point in time and space during the July 5, 7, and 8 flights, prior to cloud edge filtering. Comparisons of the mean volume radii can be found in Figure 3.2.

We examined data from the times when the aircraft was flying through and near low clouds (defined as having cloud tops at or below 220 metres) from July 5, 7, and 8, 2014. Data from these low clouds linearly correlated LWC and CDNC (see Figure 2.2), unlike when data from higher-altitude clouds or clouds containing pollution from at least one nearby ship were included (see Figure 2.1). During the flight campaign, an FSSP-100 onboard the aircraft measured the size and number of cloud droplets. The profile locations used in this study (see Table 2.1 and Figure 2.3) were determined from data from the FSSP-100. Temperature, wind speed, and relative humidity measurements from

the Aircraft Integrated Meteorological Measurement System (AIMMS-20) was also used in the creation of input profiles for the SCM-ABLC.

Date July	Start Time (UT)	End Time (UT)	Lowest Cloud Altitude Bin (m)	Highest Cloud Altitude Bin (m)	Starting Latitude	Ending Latitude	Starting Longitude	Ending Longitude
5	16:17:09	16:18:31	100	130	77.3284	77.2796	-98.7378	-98.8190
7	16:20:54	16:26:58	90	150	77.1818	77.3280	-98.4485	-98.8793
7	16:26:59	16:28:54	80	110	77.3273	77.2580	-98.8786	-98.7206
8	17:27:20	17:29:02	140	190	74.1878	74.1895	-87.8455	-88.0827
8	17:29:03	17:29:57	150	200	74.1895	74.1916	-88.0851	-88.2086
8	17:31:29	17:32:16	150	190	74.2006	74.2046	-88.4050	-88.5083
8	17:32:17	17:33:00	150	200	74.2047	74.2090	-88.5105	-88.6061
8	17:35:00	17:35:43	150	190	74.2313	74.2401	-88.8686	-88.9604
8	17:35:44	17:36:22	150	210	74.2403	74.2471	-88.9626	-89.0419
8	17:38:25	17:39:12	150	220	74.2712	74.2816	-89.3039	-89.4023
8	17:43:29	17:44:43	150	200	74.3361	74.3520	-89.9603	-90.1210

Table 2.1. Description of the location and time of the low clouds examined in this study.

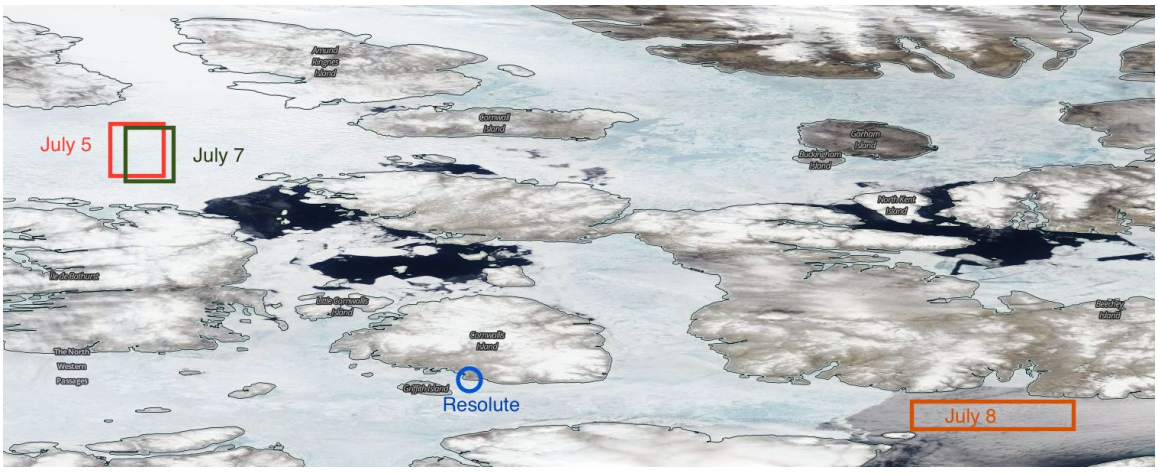

Figure 2.3 Satellite image from July 8, 2014 depicting Resolute Bay and the surrounding area, with rectangles showing the rough locations of profiles on July 5, 7, and 8. Retrieved from https://worldview.earthdata.nasa.gov/

A profile broadly contains a single trip either up or down by the aircraft and includes a section in a cloud and a few tens of metres above it. The input profiles roughly correspond to profiles in the study by Leaitch et al. (2016), but not always. We made an effort to include as many profiles as near to theirs as possible, but some of their profiles were not good fits for our model because they were from very thin cloud layers that the model could not reproduce, or were entirely within a cloud layer. As complete profiles were necessary, data were excluded when any one of the instruments collecting the data that went into the input profiles was not functioning.

2.1.3 Determining the LWC and CDNC from Measurements

The raw FSSP data was initially processed as in Leaitch et al. (2016) and further processed as described in Appendix A (Leaitch, personal communication); the result is Figure 2.2. This additional processing accounted for the geometry of the FSSP as well as programming issues with the FSSP, as the true air speed used by the instrument was incorrect (Leaitch, personal communication). No corrections were applied for probe dead-time or for coincidence effects, as these were deemed to be negligible due to the low cloud droplet number concentrations and low airspeed of the aircraft. However, LWC (and hence radii) are likely to be underestimated due to the possibility of droplets larger than the upper limits of the chosen FSSP sampling sizes, which were sometimes set below the upper detection limit of the FSSP. It is also possible that some droplets were larger than the actual upper detection limit of the FSSP, which was a diameter of 45 μm (Leaitch et al., 2016).

When modelling clouds, it is important to consider the effects of the edges of the clouds and that transition between saturated and unsaturated air. It is generally accepted that unsaturated air can be entrained into the cloud at the top and sides of the cloud as well as the bottom (e.g. Gerber et al., 2008). However, some observations of cumulus clouds have shown that the majority of the entrained air came from the cloud top region (Jensen et al.,1985). Entrained air parcels are located by the sharp gradients in LWC and CDNC on their edges – both quantities tend to be quite low in the entrained parcels compared to the surrounding cloud. Cloud droplets may also decrease in size when LWC is very small (Gerber et al., 2008). Entrained parcels have been found to exist only on scales of meters in size, and up to tens of meters into the clouds before mixing homogenizes them with the rest of the cloud (Gerber et al., 2008). As such, it is a struggle to model entrained parcels at resolutions greater than a meter. Due to these challenges, we did not examine cloud edge effects in this project.

Entrainment of dry air into the cloud and cloud edges were excluded by segregation of data points and altitude bins. LWC data points in a profile were first sorted by altitude into 10-metre bins. Next, each bin was categorized as being in cloud or out of cloud. A bin was classified as being in cloud if more than 50% of the LWC data points were greater than 0.01 g/m^3. Data points were then filtered from these bins – individual data points within each in-cloud bin were only included if their LWC was greater than 0.01 g/m^3. The same procedure was applied to altitude bins considered to be out of cloud, but individual data points needed to have a LWC less than 0.01 g/m^3 in order to be included.

Finally, each altitude bin was assigned the mean value of the LWC data points that remained. The model represents spatially-averaged conditions in the cloudy grid cells and the clear-sky grid cells separately for a better comparison of cloud to observations, where the presence of cloud is more of a binary trait, so the observed profiles chosen also excluded entrainment effects.

In our study, we assumed a constant CDNC throughout each cloud. In order to calculate the mean CDNC of the observed portion of the cloud, the CDNC corresponding to each LWC data point that went into the in-cloud altitude bins was averaged over the number of data points in that altitude bin. This accounted for potential biasing from the length of time the aircraft flew at each altitude. An average over all of the in-cloud altitude bins was then calculated as to be able to compare directly to the SCM-ABLC results, as the SCM-ABLC can only use a single input CDNC.

2.2. SCM-ABLC

2.2.1 Cloud Physics and Processes

The SCM-ABLC is based upon the fourth generation of the Canadian Atmospheric Global Climate Model (CanAM4) (von Salzen et al., 2013). Much of the model physics, from cloud processes and turbulence to the parameterizations of the ocean surface, are taken from the CanAM4. However, unlike the CanAM4, the SCM-ABLC only models liquid clouds and does not include aerosol processes. This, along with the lack of horizontal model extent, makes it less computationally intensive to run.

In the SCM-ABLC, liquid clouds form by condensation from lifting of moist air through local mixing, depending on the supply of moisture and saturation specific humidity, which is calculated from the specified temperature profile in the model. In equilibrium, evaporation of moisture is balanced by its removal through precipitation in the clouds and drying from turbulent mixing at the top of the model domain. Radiative cooling is balanced by the change in the heat flux coming from the surface.

The cloud processes in the SCM-ABLC are broadly those of the CanAM4 except the microphysics scheme only simulates warm cloud processes – ice-phase and mixed-phase cloud processes are excluded. The clouds are initialized with local mixing processes, which move moisture, heat, and momentum down-gradient, and are affected by surface fluxes (von Salzen et al., 2013). Water vapour and liquid water content are transported by vertical diffusion from turbulence. Additional details of the model can be found in von Salzen et al. (2013).

Model clouds are assumed to be homogeneous at each 10 m grid cell (von Salzen, personal communication), which allows for a straightforward comparison with the flight observations since they are over a very narrow period in time and space. Cloud microphysical processes are prognostic using a scheme that is based on the governing equations for water vapour and cloud liquid water outlined in Lohmann and Roeckner (1996) and Lohmann (1996) (von Salzen et al., 2013).

Non-local mixing, which occurs when a coherent airmass is advected a relatively large distance before being mixed with the surrounding air, is excluded in the SCM-ABLC. Eddy diffusivities calculated in the model depend on horizontal wind, height above ground, the gradient Richardson number, and a mixing length (von Salzen et al., 2013). The parameterization used to determine the mixing length if there is no cloud is based on Lenderink and Holtslag (2004), but in the presence of cloud, the mixing length is set to 100 metres (von Salzen et al., 2013). The Lenderink and Holtslag (2004) mixing length parameterization is computationally inexpensive and is computed from averaging over two integrals over stability that depend on the Richardson number. Between the surface and the altitude of the lowest initial condition, variables are calculated based on vertical diffusion with a first order turbulence closure (von Salzen et al., 2013). Surface fluxes, including evaporation from the ocean, as well as heat and momentum fluxes, are simulated using an approach based on Monin-Obukhov similarity theory, wind-speed, and gustiness (von Salzen et al., 2013). In this approach, the absolute effective wind speed is used to calculate surface fluxes; this depends on the sum of squares of the wind speed in the bottom-most model layer, the sub-cloud layer convective velocity scale, and the gustiness from deep convection (von Salzen et al., 2013).

2.2.2 Input profiles and boundary conditions

The SCM-ABLC uses the following specified meteorological variables from the aircraft observations at specified altitudes as inputs to the model: wind speed, relative humidity, LWC, CDNC, and temperature. These inputs provide upper boundary conditions for cloud simulations as well as initial conditions for the model, with the upper boundary

condition representing the beginning of the free troposphere. The lower boundary conditions at 10-metre height for temperature and pressure were specified: the surface temperature was set to 273 K as the flights were all near or over open water and ice edges and the surface pressure was set to 101325 Pa. Between the lowest observed level and the surface, the model linearly interpolated variables from the input profiles. As such, model output from this layer is considered to be less accurate than the cloud layer.

Using the LWC measurements processed as described in the observations (section 2.1.3), along with temperature, wind speed, and relative humidity measurements from the Aircraft Integrated Meteorological Measurement System (AIMMS), and the mean CDNC calculated in section 2.1.3, input profiles were created for the model runs. Only the data points corresponding to those used in the altitude bins of observed LWC and CDNC were used; these corresponded to the data points with LWC greater than 0.01 g/m^3 in cloudy altitude bins and data points with LWC less than 0.01 g/m^3 in non-cloudy altitude bins. Values of temperature, relative humidity, and wind speed associated with data points considered unrepresentative due to cloud edge or entrainment effects were excluded from these averages.

2.2.3 Boundary Layer Heights

The choice of boundary layer height is important in the SCM-ABLC since processes above the boundary layer are not well represented in the model. In order to choose the boundary layer heights, we plotted the observed and modelled LWC profiles and the observed temperature profiles in order to find the altitude of the model just above the

cloud top. The observed cloud top was identified by the height at which 50% of the LWC data points were less than 0.01 g/m^3. The observed temperature profiles were also plotted to locate the height of the base of the inversion. The boundary layer height was then chosen near the height of the base of the inversion, at the altitude which produced a LWC profile most qualitatively similar to the observations.

2.2.4 Newtonian Relaxation

Single column models can account for horizontal effects and other local effects by way of external forcings. One way to do this is by using Newtonian relaxation techniques, also known as nudging techniques. Newtonian relaxation works by assigning a relaxation coefficient that weights the model output to some given input state as a counterweight to the dependence on the model physics. Nudging can also be used to slow the growth of systematic model error; it does this by adding artificial relaxation terms to the model's prognostic equations so that the model state is nudged towards a predetermined state (Shao et al., 2016). Newtonian relaxation is also used for validation of GCM physical parameterization schemes, by nudging large-scale circulation to states determined by meteorological analyses (Jeuken et al., 1996).

The major difficulty with Newtonian relaxation techniques is determining a good choice of relaxation coefficient. If the coefficient chosen is too large, then the model results will be very close to the value getting forced to (often an observation), possibly to the detriment of model physics (e.g. dynamical imbalances can get amplified) or reality. If it

is too small, then the value getting forced to has little effect on the solution (Jeuken et al., 1996).

The model is intended to simulate processes in the boundary layer that affect cloud microphysics on short timescales (seconds to hours). As such, the SCM-ABLC uses Newtonian relaxation techniques in order to simulate the effects of processes that are not included in the model, such as horizontal advection, as well as constraining the model where processes only occur on longer time-scales. Nudging techniques are combined with the upper boundary conditions to ensure that the simulated model variables are constrained by the observed values, by setting the nudging time scale at these altitudes to be equal to the model time step (900 seconds). This ensures that the specified variables return to the input conditions at every time step, which is necessary above the boundary layer since the model is only representative where thermodynamic conditions are determined primarily by large-scale processes. This provides an upper boundary condition in the model, by providing a constant flux of moisture.

Between the lowest initial condition and the lowest upper boundary condition, Newtonian relaxation is used with varying time scales for different variables. Since advection is assumed to be less important than turbulence and cloud microphysics at these altitudes, it is possible to run the model with relatively weaker nudging. The momentum time scale was set to three hours. This allowed us to maintain realistic wind profiles but was long enough to smooth out some of the noisier wind data (short-term eddies may have been included in the observational data) and allow for more physical diffusion profiles. This

allows the model physics to account for the impacts of turbulent mixing in the boundary layer on horizontal winds, but provides a constraint to keep the model from diverging too far from realistic values. The moisture flux in the top portion of the cloud, where we examined the model output, was found to be mostly insensitive to the momentum flux at a time scale of 3 hours.

Variables	Nudging time scale
Temperature	15 minutes = model time step
Momentum	3 hours
Moisture	1E+20 seconds
All variables above nudging altitude	15 minutes = model time step

Table 2.2. The nudging time scale for different variables in the model.

The temperature was completely controlled by nudging, ensuring that the temperatures remain at the specified values according to the averaged aircraft observations. This was done to simulate water cycle processes in the model at the specified temperatures.

The nudging time scale for moisture was set to 1E+20 seconds, which allowed the model physics to completely dictate the evolution of the moisture variables. This allowed the model cloud to reach thermodynamic equilibrium for the model physics at the end of our model run. Thermodynamic equilibrium was tested for by running the model for different periods of time and examining the prognostic variables for any changes in time. The model simulation time was set to 300 hours, as this allowed the vertical integral of LWC (one of the slowest variables to equilibrate) to come to equilibrium in all cases. All cases came close to equilibrium for this variable after roughly 100 hours.

2.2.5 Autoconversion Schemes

Three different autoconversion parameterizations are implemented in the SCM-ABLC from the literature. These are described in Khairoutdinov and Kogan (2000), Liu and Daum (2004), and the modification to Liu and Daum described in Wood (2005). All of these schemes have been used in various modelling applications and were developed for the mid-latitudes. However, to our knowledge they have not been applied to summer Arctic low clouds.

The autoconversion scheme presented by Khairoutdinov and Kogan (2000) was developed to represent marine stratocumulus clouds in large eddy simulation (LES) models. This scheme, herein referred to as K&K, separates liquid water in the model into two categories: cloud water and drizzle. The scheme predicts drizzle water and drizzle drop concentration using a prognostic scheme with the cloud condensation nuclei (CCN) and supersaturation from the thermodynamics of the large-eddy scheme model (Khairoutdinov and Kogan, 2000). This scheme was found to be in good agreement with an explicit model for the two cases of no rain and heavy drizzle that were attempted (Khairoutdinov and Kogan, 2000). It is best suited and tested for conditions found in the extra-tropics and midlatitudes off the west coasts of continents where stratocumulus cloud layers arise from upwelling (Khairoutdinov and Kogan, 2000). As in the CanAM4, the K&K scheme in the SCM-ABLC has been tuned so that the rate of conversion from cloud droplets to rain drops has been increased by a factor of 2.5. This value is based on simulations with the latest version of the Canadian Atmospheric Global Climate model, CanAM4.3 (von Salzen, personal communication).

A second autoconversion scheme that was investigated is that presented by Liu and Daum (2004). This scheme, henceforth L&D, is based on the same principles as K&K, but does not assume fixed collection efficiency with respect to droplet radius (Liu and Daum, 2004). The better representation of the physics involved in the L&D autoconversion scheme results in stronger dependencies on LWC and droplet concentration (Liu and Daum, 2004). It also increases the relative dispersion (the ratio of standard deviation to the mean radius), which affects the threshold radius for autoconversion as broader distributions tend to have larger autoconversion rates (Liu and Daum, 2004). Unlike K&K, L&D has a threshold radius value before autoconversion begins, preventing rain processes below the threshold. However, it has been shown to overestimate the autoconversion rate above the threshold compared to some observations of mid-latitude marine clouds (Wood, 2005).

The final autoconversion scheme from the literature that was explored is that presented by Wood (2005), which reduced the constant term in the L&D parameterization to 12% of its original value based on a comparison with observations that showed a lower rain rate than predicted by L&D. Wood (2005) also found that the K&K scheme did not over-predict rain as much as the L&D scheme in some new test cases, and suggested that the K&K scheme may be useful in situations other than those it was designed for (Wood 2005). The modified L&D scheme (referred to as the Wood scheme) produced more realistic dependencies on cloud LWC and CDNC compared to the original L&D scheme, according to the observations that Wood compared the schemes with (2005). As Arctic

summer clouds are different from all of those tested in the past, we did our own comparison.

Two additional autoconversion schemes were included in the model for testing purposes. One was a modification of Wood (2005) that allows a constant value for the CDNC that was put in the autoconversion calculations. This scheme was used to examine the sensitivity of the combined autoconversion and cloud microphysical results to CDNC alone, eliminating the impacts of CDNC on the autoconversion rates. The final scheme added to the model for testing simulated no autoconversion by allowing the variable that represents rain water to be constantly zero, as though the threshold value for autoconversion to take place in the L&D or Wood autoconversions was never met. This allowed the SCM-ABLC to run as if all of the moisture in the clouds had to stay in either cloud droplet or vapour form. This was written into the model for diagnostic purposes, and is not in the general version of the model.

2.3. CCCma Radiative Transfer Model

2.3.1 Overview

This study uses a single column version of the radiative transfer model used in version 18 of the CanAM4.3. The radiative transfer model is described in von Salzen et al. (2013) and references therein. It solves the radiative transfer for solar and infrared wavelengths. In the context of this project, the radiative transfer calculations assume clouds to be overcast and horizontally homogeneous (von Salzen et al., 2013).

2.3.2 Model Processes

Both the solar and infrared solvers use the Monte Carlo Independent Column Approximation o account for the horizontal variability of cloud and cloud vertical overlap (Pincus, Barker, and Morcrette, 2003; Barker et al., 2008). They also both use the correlated-*k* method to model the absorption by gases (von Salzen et al., 2013; Lacis and Oinas, 1991).

The solar radiative transfer solver is a two-stream solver using the delta-Eddington approximation to calculate the radiative transfer (von Salzen et al., 2013; Zdunkowski et al., 1982). Spherical curvature and refraction of the atmosphere act on effective path length, but this is accounted for by an adjustment of the solar zenith angle from Li and Shibata (2006).

The infrared radiation solver is a two-stream solver that uses a simplified version of the solution in Li (2002), assuming overcast and horizontally homogeneous clouds to efficiently account for the scattering by cloud and aerosol particles (von Salzen et al., 2013). The small amount of solar radiation at the top of the atmosphere that falls into the category of longwave solar radiation is used as an upper boundary condition for this solver (Li et al., 2010).

2.3.3 Cloud Inputs

Specification of cloud properties are necessary inputs to the radiative transfer model. The model requires as input the effective radius, liquid water path (LWP), cloud fraction, and

cloud heights. We input the same thickness of cloud as was observed by the NETCARE flights, which allowed us to compare corresponding longwave and shortwave radiation from the clouds modelled from the observed clouds and those modelled by the SCM-ABLC. If we did not do this, the optical depths of the modelled clouds would differ from those of the clouds based on observations simply based on cloud thickness, but we wanted to compare radiative differences due to model output. As such, we used the LWC and effective radii output from the SCM-ABLC from the top altitude bins with cloud for the same thickness as the observed cloud. The LWC was then multiplied by the bin height to yield the LWP needed as an input to the radiative transfer model. The cloud fraction was set to 1 at the altitudes from which the LWC and effective radii were taken in the SCM-ABLC.

2.3.4 Surface Albedo

It is impossible to discuss the solar radiative effect of clouds in the atmosphere without considering the surface albedo, which is a measure of the reflectivity of the surface (reflected solar radiation compared to the incoming), over which they occur. The surface albedo also determines the importance of the cloud radiative effect, since clouds and ice often have similar albedo values but the ocean surface is much less reflective of incoming solar radiation. As such, the presence of cloud over open water has a much larger radiative change than the presence of cloud over ice. Satellite data from July 5 and 7, 2014 shows that seasonal sea ice was present below the cloud, while the cloud measured on July 8, 2014 was over open water (see Figures 2.4-2.6).

Figure 2.4. Location of the plane during the observations on July 5, 2014. Retrieved from https://worldview.earthdata.nasa.gov/

Figure 2.5. Location of the plane during the observations on July 7, 2014. Retrieved from https://worldview.earthdata.nasa.gov/

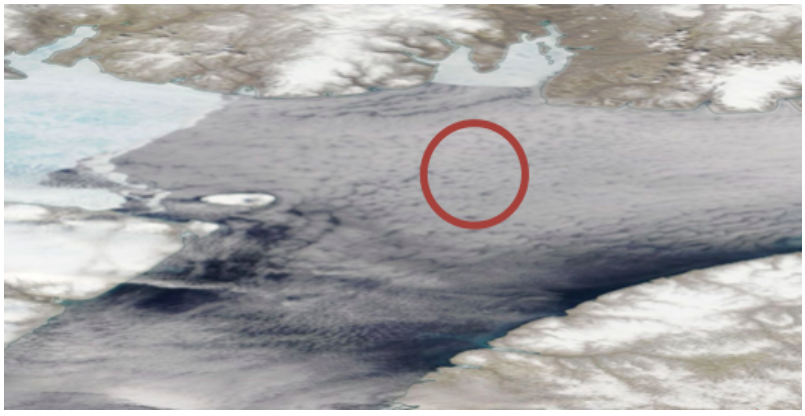

Figure 2.6. Location of the plane during the observations on July 8, 2014. Retrieved from https://worldview.earthdata.nasa.gov/

Ocean surfaces are relatively dark and therefore reflect less solar radiation. As such, the values of oceanic surface albedos tend to be low, with dependence on parameters such as wind speed and solar angle (Li et al., 2006). Many parameterizations have been written to try to best describe the oceanic albedo in various climate models (Li et al., 2006). In some of these schemes, the albedo values only depend on the solar angle, and are averaged over long sets of observations under different sea states (Li et al., 2006). The parameterization that we used falls into this category and is described below.

The parameterization for ocean surface albedo we used uses a relationship for clear-sky surface albedo that depends only on the solar zenith angle, which was derived from the aircraft locations during the profiles. Tests by Taylor et al. (1996) showed that the observations varied from the modelled relationship by only 3% over the range of clear-sky conditions for this parameterization. The ocean surface albedos varied significantly in a comparison between this parameterization and a few others; according to Li et al. (2006), the results of using the parameterizations in a one-dimensional radiative transfer model varied less, and the result of using the parameterizations in global climate models and averaging over five years produced similar results as the one-dimensional radiative transfer models.

From the Taylor et al. (1996) parameterization of the surface albedo on July 8, we obtained a value of 0.054 based on the solar zenith angle at the time of the flight. Many other parameterizations have found ocean albedos to average 0.06 worldwide. Examining the effect of high-latitudes on the parameterization by decreasing the solar zenith angle, it

was apparent that solar zenith angles closer to 90 degrees resulted in much higher ocean albedos, so a slightly lower than average albedo value for locations in the Arctic seemed reasonable. This albedo value was used for all wave numbers.

The last decade has seen a large decrease in the amount of multi-year sea ice in the Arctic, which has mostly been replaced by seasonal ice and open water (Perovich and Polashenski, 2012). To account for the presence of sea ice on July 5 and 7, we used a parameterization that accounts for the lower surface albedo values of seasonal ice, compared to multi-year ice. It also accounts for the difference in the albedo of seasonal sea ice based on observations of the various stages of melt and freeze-up by Perovich and Polashenski (2012).

These seasonal ice albedo values cannot generally be observed by satellites due to the persistence of cloud cover in the summer Arctic (Perovich and Polashenski, 2012). Seasonal ice albedo values are similar to multi-year ice albedo values before the melt season, but consistently lower than multi-year ice albedo values during the melt and freeze-up seasons due to additional warming of the flatter, thinner ice (often resulting in total melt) and the presence of nearby water, including melt ponds and leads (Perovich and Polashenski, 2012). This may affect the warming or cooling potential of clouds above the ice.

We assume from studying Figures 2.4 and 2.5 along with the melt extent on other days in July 2014 that melt had not yet started over the location of the flight on July 5, but that it

was underway by July 7. We made the approximation that there had been one day of melt for the albedo calculation on July 7. Perovich and Polashenski (2012) estimate the visible albedo of snow before melt begins to be 0.85, which is high compared to some estimates, but within the realm of observations. With these assumptions and the solar zenith angles at the times of flight, we obtained albedo values of 0.85 on July 5 and 0.81 on July 7 based on the procedure described by Perovich and Polashenski (2012). These albedo values were again used for all wave numbers. These albedo values are higher than many estimates of ice albedos, but there is a large range of measured and modelled values for ice albedo, with some estimates running from 0.5 to 0.9 (Curry et al., 1996; Sedlar et al., 2010).

2.3.5 Other Inputs and Model Configurations

Additional inputs and assumptions are needed to compute the radiative transfer. The model was run from 20 metres altitude to over 88 kilometres. Aerosols were not included in the radiative transfer calculations as we wanted to only examine the cloud effects due to liquid water, CDNC, and effective radii changes.

The pressures and initial temperature profiles at all atmospheric levels in the model were determined by interpolating the reanalyses provided by the European Centre for Medium-Range Weather Forecasts (ECMWF) nearest the time and location of profiles. We used the ECMWF Re-Analysis (ERA)-Interim product. The retrieval of reanalyses and interpolation to the model height levels were carried out by Dr. Rashed Mahmood, who compiled files containing pressure and temperature at all model levels. The entire initial

temperature profiles were then scaled by a coefficient comparing the mean reanalyzed cloud temperatures to the mean observed cloud temperatures so that the cloud temperatures in the profiles were closer to the observed. The different times of the reanalyses and flights may have contributed to the differences, but another part of these differences can likely be attributed to the sparsity of weather data in the Arctic. The surface skin temperature was chosen by rounding the temperature interpolation at the lowest level to the nearest degree.

Dr. Rashed Mahmood also compiled the input files containing values at each model level for mixing ratios of carbon dioxide, methane, nitrous oxide, CFC-11, CFC-12, water vapour, ozone, and carbon tetrachloride from the trace gas climatologies used in the ECMWF Integrated Forecasting System. Carbon monoxide and oxygen mixing ratios were not included in the model.

CHAPTER 3 RESULTS AND DISCUSSION

3.1. Observations

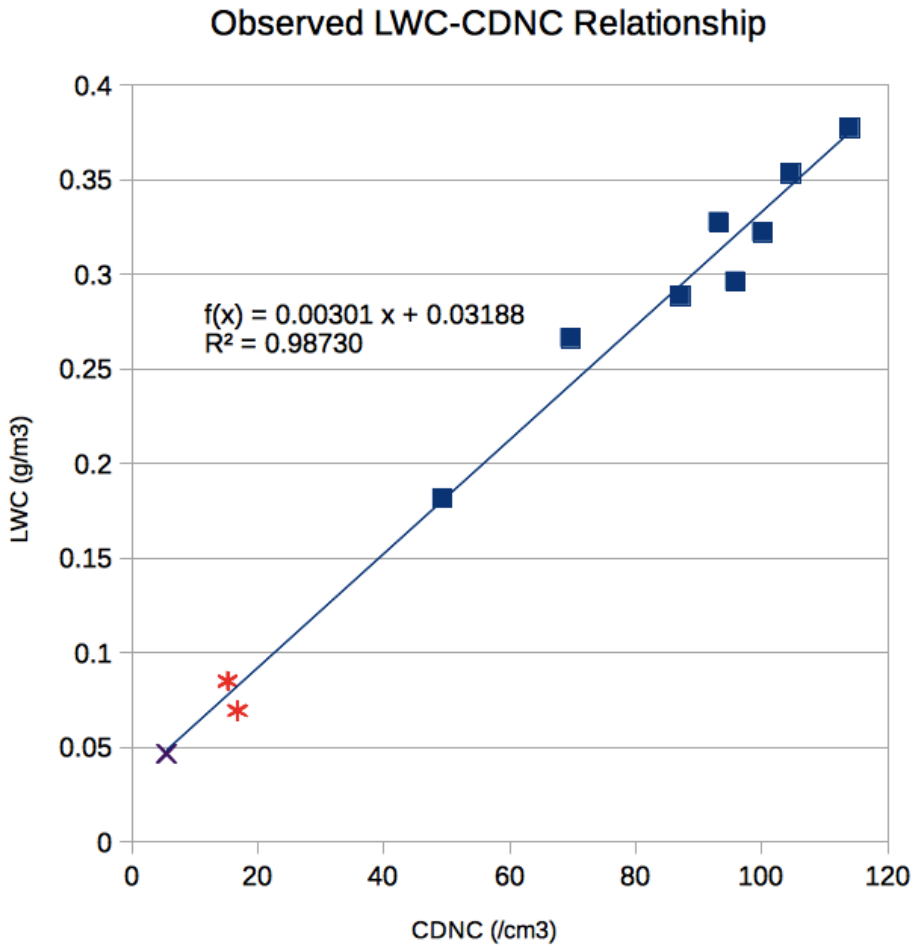

Figure 3.1. Averaged liquid water content to averaged cloud droplet number concentration in each profile taken from observations during the July 5, 7, and 8, 2014 flights (purple X, red asterisks, and blue squares, respectively), as described in section 2.1. The relationship between the LWC and CDNC appears to be linear.

In order for a profile to be considered in the model, it needed to have at least 20 metres of data both in the cloud and above the cloud top, so the observations corresponded to times during which this occurred (as discussed previously in section 2.1). However, Figure 3.1

only includes LWC and CDNC data from when the aircraft was in cloud. Similar to the results from Leaitch et al. (2016), there appears to be a linear relationship between the CDNC and LWC. The variance is low, with $R^2 = 0.987$. This result resembles the plot of LWC to CDNC over different time periods in Leaitch et al. (2016), which did not require that there be vertical profiles of the two, but only included clouds with tops below 200m. This linearity suggests that the mean volume radii ought to be similar over the various profiles, and they are indeed fairly similar, as seen in Figure 3.2.

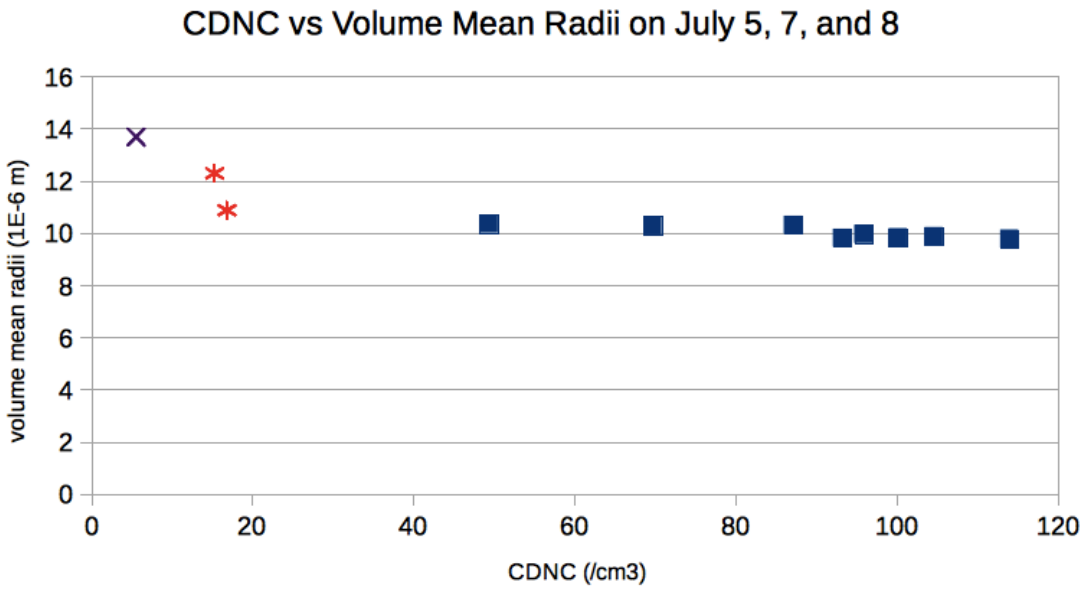

Figure 3.2. Effective radii calculated from profile-averaged observations of LWC and CDNC during the July 5, 7, and 8, 2014 flights (purple X, red asterisks, and blue squares, respectively). The radii do not seem to depend strongly on CDNC at concentrations above 20/cm^3, and are still similar even at lower CDNC.

3.2. SCM-ABLC

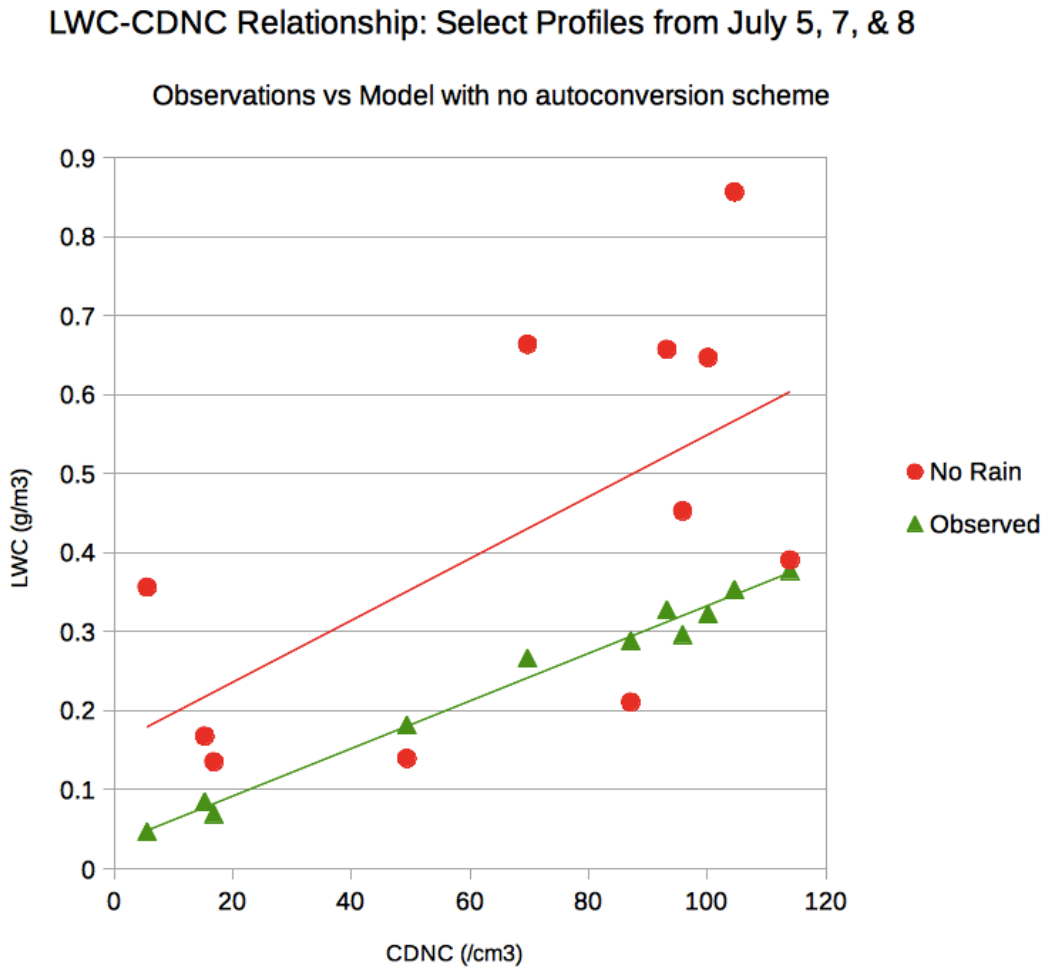

Figure 3.3. LWC resulting from the SCM-ABLC run with no autoconversion scheme, is not as linear as the observed LWC when sorted by CDNC.

We tested whether the SCM-ABLC could produce the relationship between LWC and CDNC with no autoconversion scheme. Figure 3.3 shows the observed LWC to CDNC relationship from Figure 3.1 (in green triangles), along with the results of a model run with no autoconversion scheme (hence no cloud water turning to rain). The model run with no autoconversion scheme has greater variance, a steeper slope, and an offset for larger LWC compared to the observations (see "No Rain" case in Table 3.1 for slope and R^2). This suggests that an autoconversion scheme is necessary to simulate the observed

linearity between LWC and CDNC, as it appears that the model retains too much water otherwise. This demonstrates that mixing is not the primary cause of the linearity in the observations, provided that mixing is properly represented in the model and over the profile average, which we do believe.

	Slope	R^2	Intercept
Observations	0.00301	0.987	0.03188
Wood	0.00353	0.554	0.06670
L&D	0.00290	0.736	0.04489
K&K	0.00388	0.707	-0.01621
No rain	0.00391	0.387	0.15796
L&D and K&K	0.00330	0.795	0.04153
Constant 5/cm^3	0.00187	0.512	0.12697
Constant 112/cm^3	0.00311	0.443	0.15620

Table 3.1. Slopes, coefficients of determination, and intercepts for all of the modelled LWC to observed CDNC. 'Observed' corresponds to the relationship from the observed LWC to the observed CDNC. 'Wood,' 'L&D,' and 'K&K' correspond to the LWC produced by the model runs with those autoconversion schemes. 'No rain' corresponds to the LWC produced by the model with no autoconversion scheme. 'L&D and K&K' corresponds to the combination of L&D and K&K schemes so as to use the K&K scheme at CDNC < 20/cm^3 and the L&D scheme at higher CDNC. 'Constant 5/cm^3' and 'Constant 112/cm^3' refer to the test cases of the Wood scheme that were run with all of the profiles having constant CDNC of 5/cm^3 and 112/cm^3, respectively.

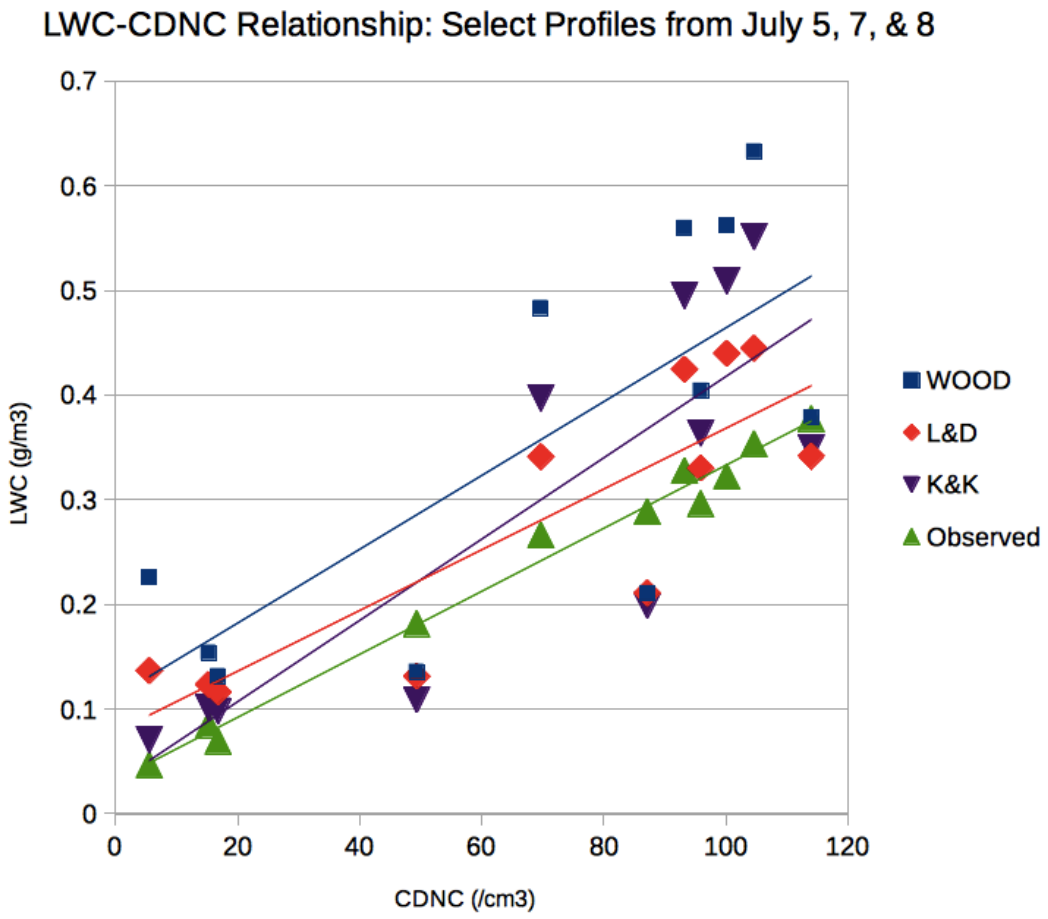

Figure 3.4. LWC to CDNC from the observations and the three autoconversion schemes tested in the SCM-ABLC.

Figure 3.4 shows that the tested autoconversion schemes seem to over-predict the LWC compared to observations in most cases, but succeed in capturing some of the linearity present in the observations. The two cases for which the model under-predicts the LWC appear to have less liquid water in the boundary layer, specifically at cloud height, as well as lower wind speeds than some of the other profiles, which may have influenced the modelled LWC. Our main goal was to recreate the linear relationship observed between the LWC and the CDNC. The Wood scheme is the most variable and over-predicts the observations most. The K&K scheme has the largest slope but over-predicts the least at

lower CDNC, while the L&D scheme has the smallest slope and over-predicts the observations the least at higher CDNC. Overall, the L&D scheme does best at higher CDNC, while the K&K scheme does best at lower CDNC, in comparison with the observed LWC. The slopes and variance in Table 3.1 show that the L&D scheme outperformed the Wood scheme in both measures, suggesting that the adjustments for decreased autoconversion made by Wood to the original L&D autoconversion scheme are not suitable for the Arctic. The K&K scheme is closest to the observations at low CDNC, which may account for the higher sensitivity of LWC to CDNC at very low number concentrations, as the continuous conversion of cloud droplets to rain drops with no threshold before conversion begins may be a better representation of reality at these low CDNC. Overall, it seems that the autoconversion needs to maintain an effective radius of roughly 10 micrometres in order to match the observations.

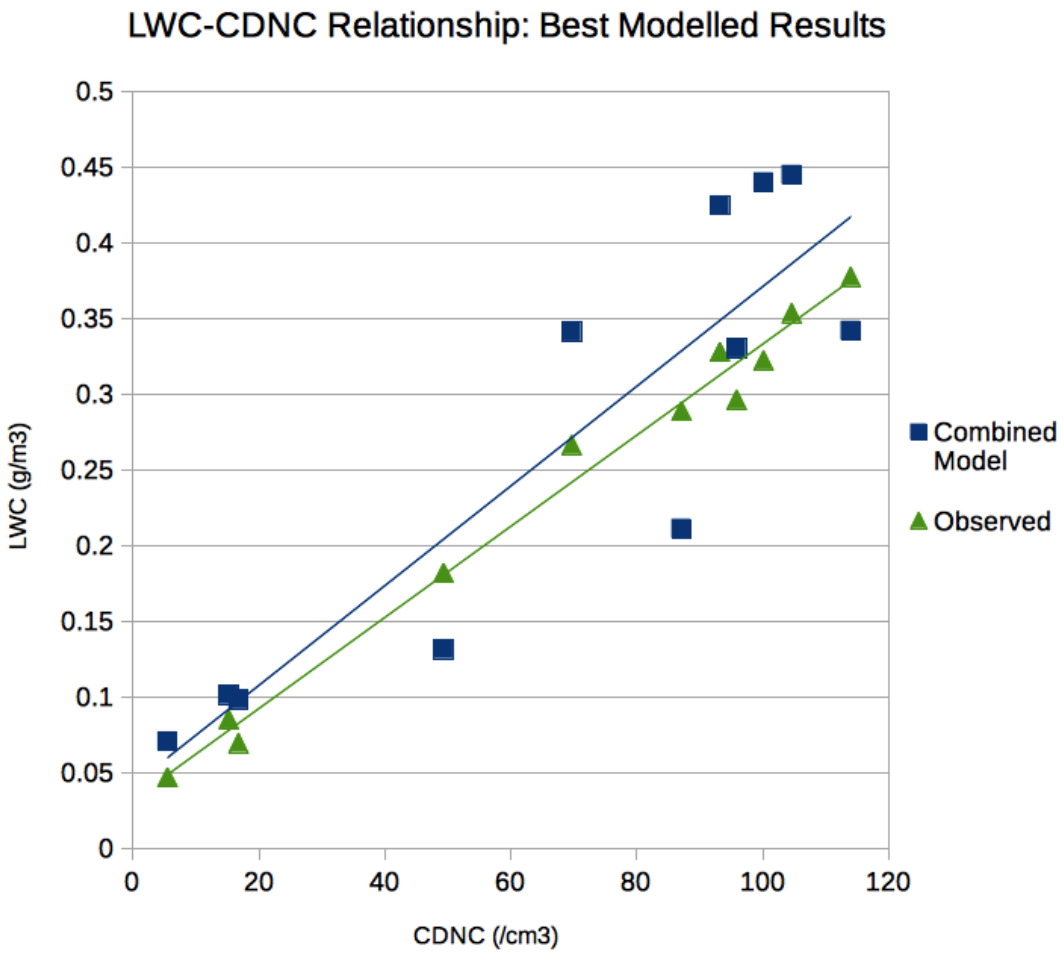

Figure 3.5. Observed LWC to CDNC relationship with a combination of the K&K and L&D schemes, using the K&K scheme at low CDNC and the L&D scheme at higher CDNC.

We tried to capture the strengths of these two schemes by combining the L&D and K&K schemes as follows: we used the K&K scheme to model the three profiles with CDNC below 20/cm^3 and the L&D scheme for the rest, as the K&K scheme does best at modelling the LWC at low CDNC, while the L&D scheme does best at high CDNC. Figure 3.5 shows the result of this combination of schemes. It does the best at obtaining a smaller variance and the overall slope is similar to the observations, as seen in Table 3.1. The comparison of modelled to observed results show a change of regime occurring

around 20/cm^3, which is near the Mauritsen limit of 10 CCN/cm^3 and the changes to the limit proposed by Leaitch et al. (2016), which suggested that as the Mauritsen limit reflects more of a change in regime than a specific numerical cutoff, the numerical cutoff may be different at various locations and times. The numerical limit suggested by Leaitch et al. (2016) was 16/cm^3. The K&K scheme doing best at CDNC below 20/cm^3 but the L&D scheme doing best for higher CDNC is suggestive of a regime change like that described by the Maurtisen limit. This may be due to the lack of a threshold for drizzle production in the K&K scheme which is present in the L&D scheme, corresponding to the speed at which droplets grow large enough to fall at low CDNC compared to higher CDNC. Other models may also need to consider regime changes that occur in the observations in order to better represent reality.

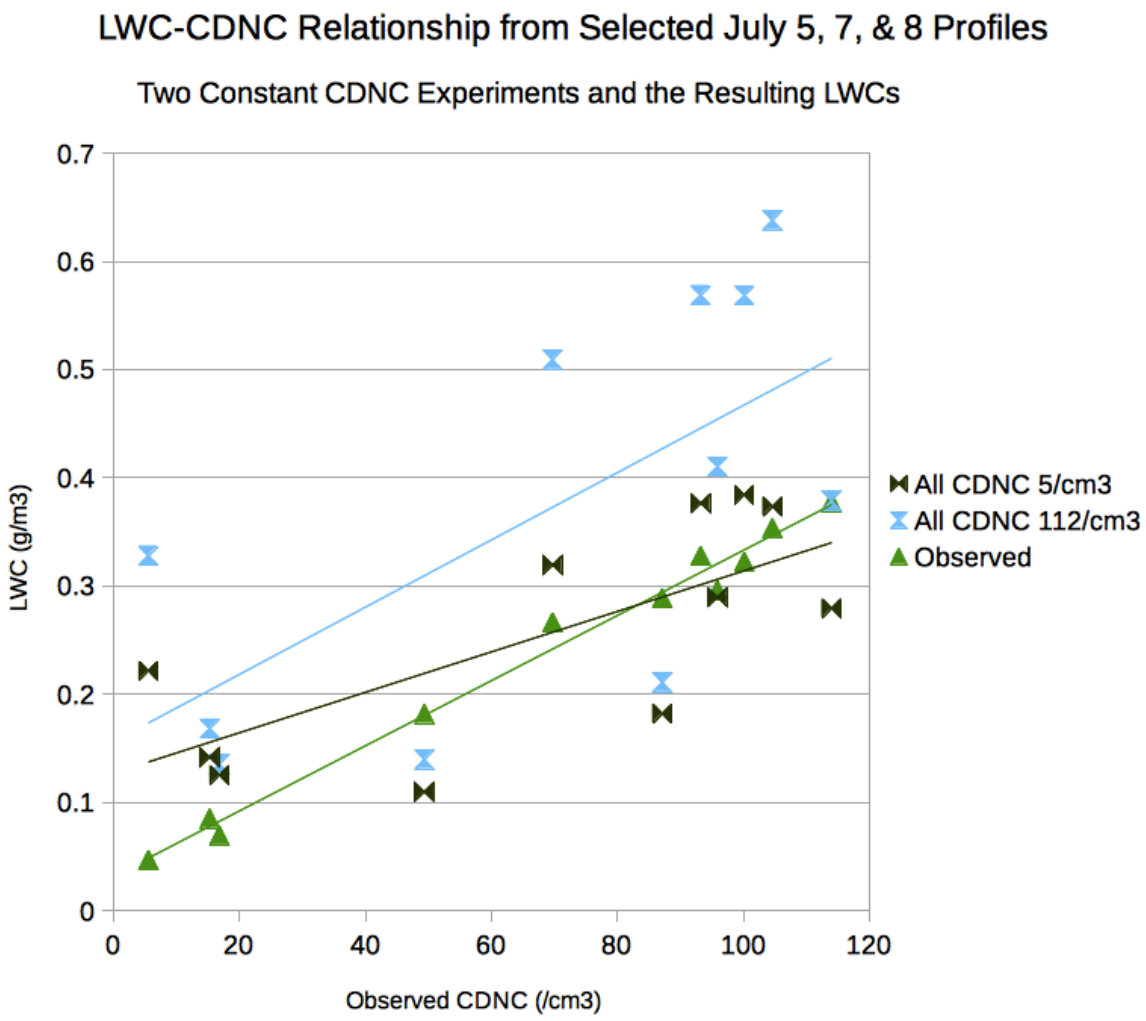

Figure 3.6. A comparison of the LWC from observations with LWC resulting from the SCM-ABLC run with constant values of CDNC (5/cm^3 and 112/cm^3) for all profiles. The model runs have much higher variance.

In order to determine the effect of other parameters on LWC besides CDNC, we kept the CDNC constant while leaving the variation in temperature, relative humidity, and wind speeds in the input profiles. We chose the highest and lowest observed CDNC values (5/cm^3 and 112/cm^3) to see the amount of variation created by the CDNC as well. Figure 3.6 shows these results. It should be noted that the x-axis is not representative of the CDNC from this run but rather from the measured CDNC of each profile. The model runs

with constant CDNC have much higher variance than the observations (see Table 3.1). In addition, the variances of these model runs and the intercepts are larger than the model runs where CDNC is allowed to vary between profiles. If CDNC were the only driver, there would be a horizontal line as the relationship between LWC and CDNC, but Figure 3.6 and Table 3.1 show this is not the case. This shows that the relationship between the LWC and the CDNC is not solely dependent on the autoconversion rates. Other dependencies likely include temperature and wind speed profiles.

One major shortcoming of our approach is the use of a single mean value of CDNC for each cloud profile. The autoconversion schemes were not intended for single values of CDNC everywhere in the modelled cloud, and the observations had at minimum a range of 8/cm^3 and up to standard deviations of over 30/cm^3 over the profiles. Nevertheless, the average modelled LWC values correspond well with the observations, and the relationship between LWC and CDNC appears to be preserved in the model.

Other studies have previously noted that autoconversion schemes often do not represent the rain rates of the Arctic very well (Croft et al., 2016; Zhang et al., 2002; Olsson et al., 1998). Olsson et al. (1998) speculated that the discrepancy between modelled and observed rain rates may be due to the size of droplets, as small droplets can fail to initialize autoconversion when the threshold is too large. Our results support this theory at low CDNC: the K&K scheme, which has no threshold for autoconversion, does best at low CDNC, suggesting that the thresholds for autoconversion may be too high in the L&D and Wood schemes at these droplet concentrations. However, we find that the L&D

scheme does best at higher CDNC, so there may be a regime change associated with this issue.

3.3. Radiation

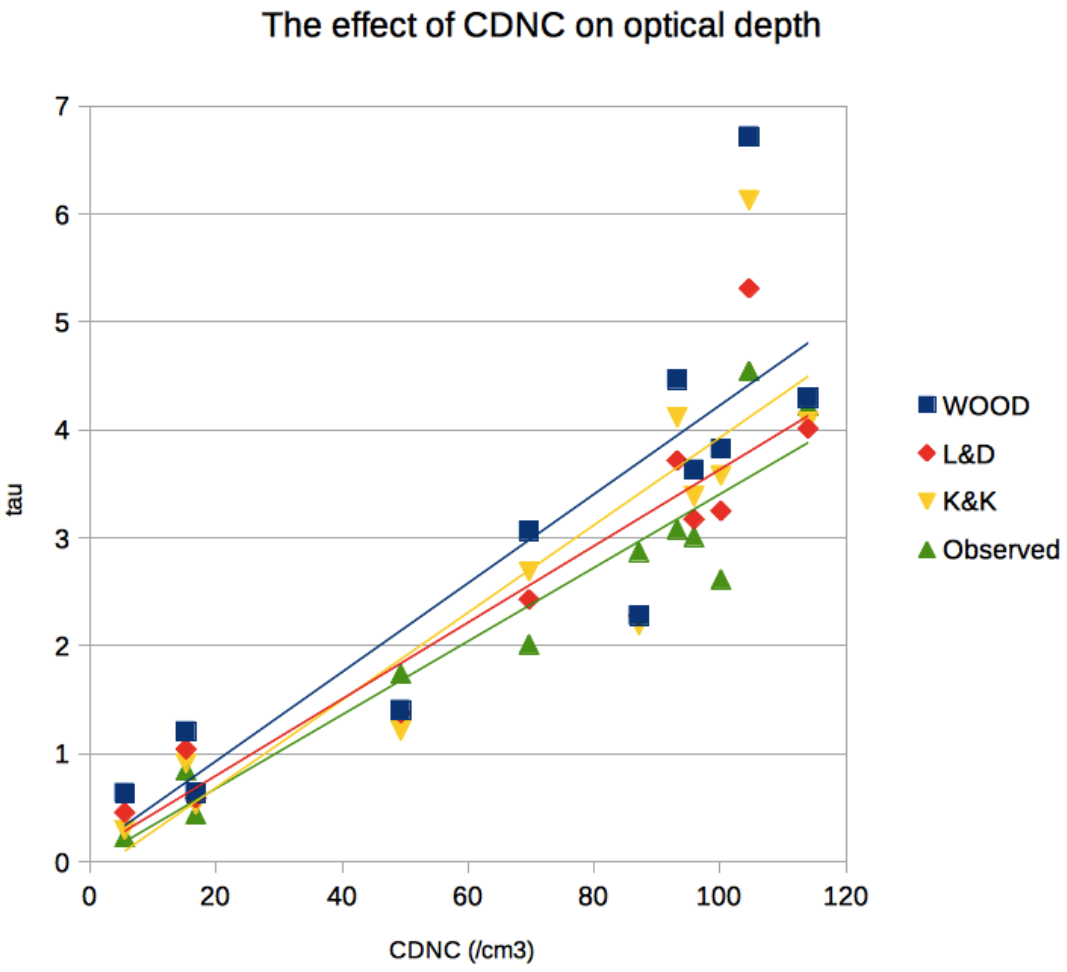

Figure 3.7. Optical thickness of the cloud calculated from observed LWC, cloud thickness, and CDNC.

The observed optical thickness, shown as tau in Figure 3.7 is a calculation from observations, not a direct measurement. The calculation is the result of assuming the

cloud to be a plane-parallel layer, and results in $\tau = Q_e[\frac{9\pi L^2 H N}{16\rho_l^2}]^{\frac{1}{3}}$, where L is the liquid water path, H is the thickness of the cloud layer, N is the cloud droplet number concentration, Q_e is the extinction efficiency, and ρ_l is the density of liquid water (here assumed to be 1000 kg/m^3). To calculate the extinction efficiency, we examined the size parameter. For the size parameter to equal 1, that is, $x = \frac{2\pi r}{\lambda} = 1$, where r is the radius and λ the wavelength, a radius of 2 μm was necessary for a wavelength of 12 μm and the radius required to maintain this size parameter decreased for shorter wavelengths. The observed volume mean radii were generally 10 μm or larger (see Figure 3.2), so the size parameter was large enough for the extinction efficiency to be approximated as 2. As we found a linear relationship between the LWC and CDNC, and LWP is simply the vertical integration of LWC over some altitude, $\tau \propto [N^3]^{\frac{1}{3}}$ and so the optical thickness ought to be linearly related to the CDNC. The same thicknesses of cloud were used in the observed and modelled cases since the thickness of the observed clouds could not be measured due to limitations of the sampling method. As such, the thickness from the top of the cloud to the bottom of the observed profile is used for both the observed and modelled clouds.

The optical depth calculated from the modelled variables is generally higher than that calculated from the observed variables, due to the generally higher values of liquid water produced by the model, however, they are similar. The L&D scheme performed best

overall at reproducing the calculated optical thicknesses from the observations, and the Wood scheme is furthest from the result based on observation.

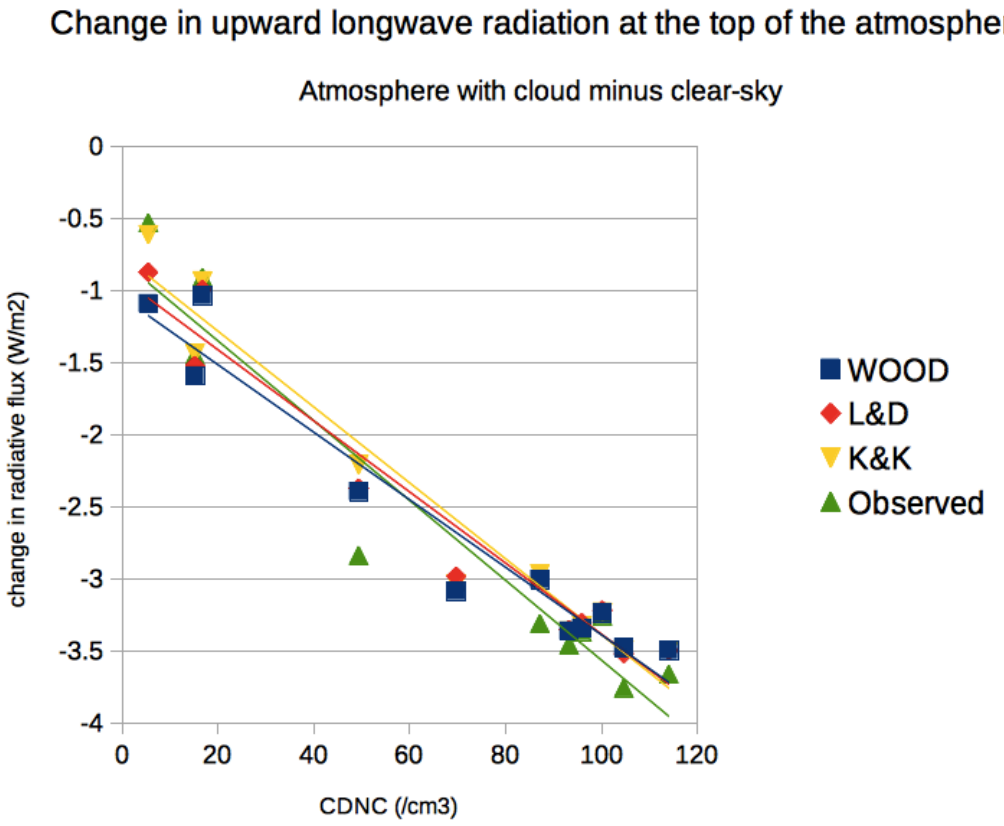

Figure 3.8. Change in upward longwave radiation at the top of the atmosphere due to the presence of cloud, wherein the input cloud variables were from the SCM-ABLC output.

The CCCma Radiative Transfer Model, version 18 was run with cloud inputs of liquid water path and effective radius from the SCM-ABLC. All of the surface albedos were set to be such that this was over open water, but the differences in solar insolation from the different days were included. Figure 3.8 shows that there appears to be a small offset at values of CDNC greater than 20/cm^3 between the longwave radiation at the top of the atmosphere from the model run with observed liquid water path and effective radius and

the model run with the results from the SCM-ABLC (see Figure 3.8). It also appears that the change in the radiative flux due to the presence of cloud and the CDNC of that cloud is linearly decreasing. Further, there appears to be no significant difference at p=0.01 in the radiative effect due to the cloud between the autoconversion schemes and the observation-based model run on July 8. There is also no significant difference between the different autoconversion schemes (see Table 3.2). July 5 and 7 data were not included in this comparison due to the different solar zenith angles during those flights, and to exclude the possibly different regime below 20/cm^3.

Upward longwave flux: TOA	L&D	K&K	Observed
WOOD	0.23684	0.16937	0.03555
L&D	-	0.49965	0.01317
K&K	-	-	0.03783

Table 3.2. t-test results for the change in the upward longwave radiation at the top of the atmosphere due to the clouds from the results of the CCCma Radiative Transfer Model, version 18 with LWC and effective radii inputs for the Wood, L&D, and K&K cases taken from the SCM-ABLC output for July 8, 2014.

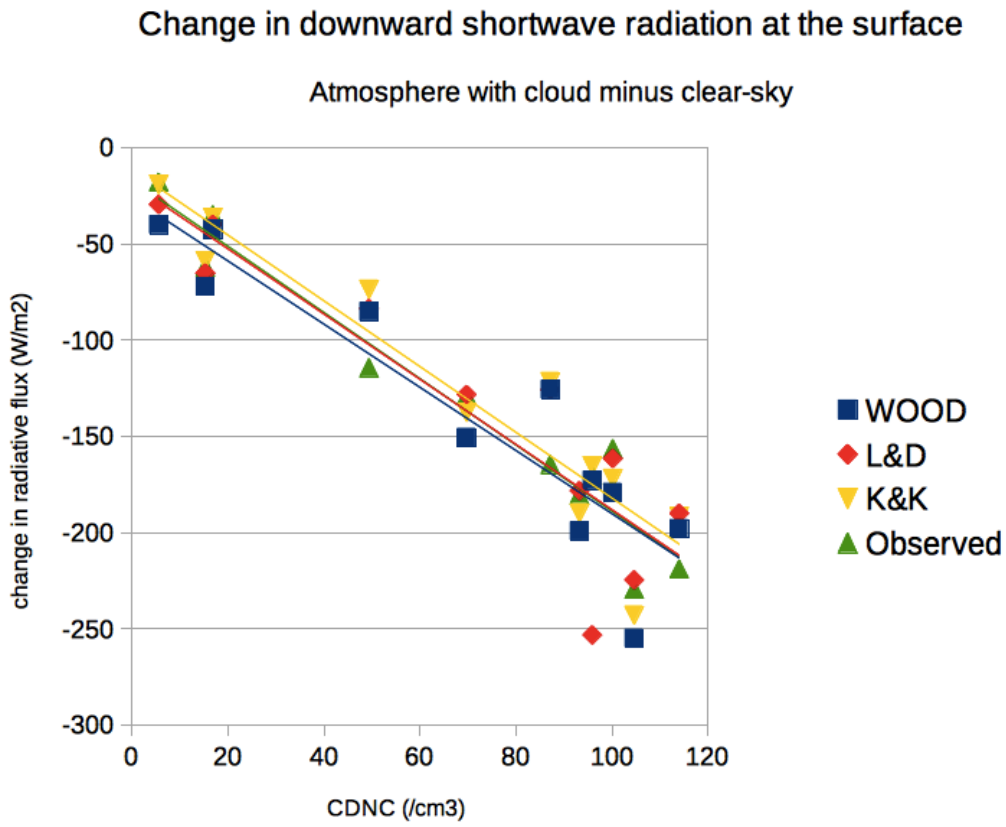

Figure 3.9. Change in downward shortwave radiation at the surface due to the presence of cloud, wherein the input cloud variables were from the SCM-ABLC output.

Similar results are seen in the downward shortwave radiation at the surface. However, there does not appear to be any offset between the radiation calculated from observations and from the SCM-ABLC output (see Figure 3.9). It still appears that there is a fairly linear relationship between the change in the downward shortwave radiative flux due to the presence of cloud and the CDNC of that cloud (see Figure 3.9). Further, there appears to be no significant difference at p=0.01 in the downward shortwave radiative effect at the surface between each scheme and the observation-based model runs on July 8. However, there is a significant difference between the Wood and other autoconversion schemes (see Table 3.3).

Downward shortwave flux: surface	L&D	K&K	Observed
WOOD	0.00623	7.795E-5	0.97484
L&D	-	0.13721	0.04520
K&K	-	-	0.35288

Table 3.3. t-test results for the change in the downward shortwave radiation at the surface due to the clouds from the results of the CCCma Radiative Transfer Model, version 18 with LWC and effective radii inputs for the Wood, L&D, and K&K cases taken from the SCM-ABLC output for July 8, 2014.

T-tests were conducted on the July 8 radiative transfer model output. Focussing on only the July 8 output allowed us to disregard the effects of different solar zenith angles on the results, as the observations were close enough in time to be approximated by the same solar zenith angle. However, there are a few considerations to be wary of, particularly the assumption of independence needed to conduct t-tests. We argue that enough independence is gained through the model runs of different profiles that the average radiative output between the profiles ought to not violate the assumption. This is because while the SCM-ABLC uses the same input profiles for each set of cases, different autoconversion schemes were used. More independence is gained as only the top parts of the modelled clouds (resulting from the different autoconversion schemes) are used as inputs to the radiative transfer model. The variables in the t-test being examined are the result of two separate model runs, the first of which uses different rain processes. We argue that this is sufficient independence to consider a t-test valid. The t-tests compare the means of the results of the radiative transfer model output.

A few main conclusions come forth from the t-tests on July 8, with perhaps the most significant to the SCM-ABLC being the revelation that using the model output effective radii results in an offset between the radiative calculations based on the observations and those based on the model output for the upward longwave radiation at the top of the atmosphere which is significant at p=0.05 but not at p=0.01. However, all three autoconversion schemes produce radiative results that are not significantly different (p=0.01) from the radiation calculated from the observations for both the upward longwave radiation at the top of the atmosphere and the downward shortwave radiation at the surface. A final takeaway from the t-tests was that the Wood autoconversion produced significantly different downward shortwave radiation at the surface from the other two autoconversion schemes at a significance of p=0.01; the L&D and K&K schemes did not significantly differ from each other.

CHAPTER 4 CONCLUSION

The choice of autoconversion in the SCM-ABLC results in different LWC output by the model. The best simulation of the relationship (chosen by the lowest variance) between the LWC and CDNC that we found was to use the K&K scheme at CDNC below 20/cm^3 and the L&D scheme above it. These two autoconversion schemes were chosen for those regimes by examining how close the data points in each section were to the observations. There seemed to be a regime change between very low CDNC and higher CDNC, which corresponds to the Mauritsen limit. This may be due to the better fit of the constantly-drizzling K&K scheme, compared to the L&D and Wood schemes which have a threshold radius for drizzle to occur, resulting in droplets growing and falling out faster at low CDNC. It may be of interest to further study the distinction between the possible different regimes of very low CDNC and how these CDNC regimes effect cloud properties. The K&K autoconversion scheme did best in this regime, but we were unable to examine the cutoff above which the L&D scheme did best, due to a lack of observational data. It would be of interest to examine if the cutoff CDNC can be reproduced in models, as the observational data showed that cloud properties such as effective radius varied between the regimes.

The radiative impacts of the modelled variables using all three autoconversion schemes did not differ significantly at p=0.01 from those due to the observations, as calculated by the CCCma Radiative Transfer Model, version 18. However, the Wood autoconversion scheme produced downward shortwave radiation at the surface significantly different

(p=0.01) from the K&K and L&D schemes. This appears to be due to the difference in the modelled LWC in the Wood scheme as compared to the K&K and L&D schemes, and indicates that the Wood scheme may be less suitable for modelling low clouds in the summer Arctic, which tend to have low CDNC. The Wood scheme still did not cause the t-tests to reject the hypothesis of equal means with the radiation calculated from observations that we examined for the July 8 cases, however, so it is not entirely unsuitable. The choice of autoconversion scheme becomes more relevant when examining the cloud microphysical properties for their own sake, and for this the combination of K&K and L&D schemes should be used. When the autoconversion scheme is only an intermediate step before obtaining the radiative effects of the cloud, however, this study did not find a significant difference between K&K or L&D schemes. The Wood autoconversion scheme produced radiative results that were significantly different from the K&K and L&D schemes, which were previously qualified as better at reproducing the linear relationship between CDNC and LWC, and so while the Wood scheme did not produce radiative results that were significantly different from those calculated from observation at p=0.01, this study recommends the use of L&D or K&K autoconversions over that of Wood.

Future work should include testing to determine if the relationship between LWC and CDNC continues throughout the full thickness of the clouds, perhaps by way of a combination of drones, tethersondes, more flight campaigns, and measurement towers on the ground. Another point of interest would be to determine the relative frequency in which the linear relationship between LWC and CDNC occurs, and whether the model

can also simulate it under other observed conditions. Whether or not the relationship is present throughout the entire cloud, it would be worthwhile to examine whether models can reproduce the observed relationships, as relatively little is known about thin low clouds in the summer Arctic. As part of this future work, radiative transfer calculations could again be carried out on both the observed and the modelled simulations of the clouds. There remain large uncertainties in the radiative effect of low clouds in the summer Arctic, and ensuring that cloud microphysical properties are being well-represented in models is one way to begin to reduce that uncertainty. Another important component of reducing the uncertainty in the radiative effect of clouds like these in the summer Arctic involves comparing the calculated radiative effect to observations. Remote sensing or in-situ observations would allow us to gather observations in order to test if our modelled cloud radiative effects are accurate.

It would be interesting to examine whether the radiative effects of the clouds is different below and above the Mauritsen limit, however, we did not have sufficient data below the Mauritsen limit for this to be robust. More data from future flight campaigns like this one would be necessary, as few profiles of cloud microphysics exist when the CDNC is so low.

It is possible that the linearity between the LWC and CDNC is present in clouds that are relatively clean in other locations. Marine regions are known for having relatively low CDNC as well. It would be interesting to learn from similar flight campaigns over mid-latitude oceans if the same type of linear relationship exists, and whether attempts to

model these clouds would result in the same autoconversion parameterizations being more representative.

REFERENCES

ACIA, 2005. Arctic Climate Impact Assessment. ACIA Overview report. Cambridge University Press. 1020 pp.

Barker, H. W., Cole, J. N. S., Morcrette, J.-J., Pincus, R., Räisänen, P., von Salzen, K., & Vaillancourt, P. A. (2008). The Monte Carlo Independent Column Approximation: An assessment using several global atmospheric models. *Quarterly Journal of the Royal Meteorological Society*, *134*, 1463-1478.

Coelho, A. A., Brenguier, J., & Perrin, T. (2005). Droplet spectra measurements with the FSSP-100. part I: Low droplet concentration measurements. *Journal of Atmospheric and Oceanic Technology, 22*(11), 1748-1755. 10.1175/JTECH1817.1 Retrieved from http://search.proquest.com/docview/222498939

Croft, B., Martin, R. V., Leaitch, W. R., Tunved, P., Breider, T. J., D'Andrea, S. D., & Pierce, J. R. (2016). Processes controlling the annual cycle of arctic aerosol number and size distributions. *Atmospheric Chemistry and Physics, 16*(6), 3665-3682. doi:10.5194/acp-16-3665-2016

Curry, J. A., Schramm, J. L., Rossow, W. B., & Randall, D. (1996). Overview of Arctic cloud and radiation characteristics. *Journal of Climate, 9*(8), 1731-1764. 10.1175/1520-0442(1996)0092.0.CO;2

Gerber, H. E., Frick, G. M., Jensen, J. B. & Hudson, J. B. (2008). Entrainment, mixing, and microphysics in trade-wind cumulus. *Journal of the Meteorological Society of Japan, 86*(A), 87-106.

Gultepe, I. (2007). *Fog and boundary layer clouds*. Basel [u.a.]: Birkhäuser.

Jensen, J. B., Austin, P. H., Baker, M. B., & Blyth, A. M. (1985). Turbulent mixing, spectral evolution and dynamics in a warm cumulus cloud. *Journal of the Atmospheric Sciences, 42*(2), 173-192. TMSEAD>2.0.CO;2

Jeuken, A. B. M., Siegmund, P. C., Heijboer, L. C., Feichter, J., & Bengtsson, L. (1996). On the potential of assimilating meteorological analyses in a global climate model for the purpose of model validation. *Journal of Geophysical Research: Atmospheres, 101*(D12), 16939-16950. 10.1029/96JD01218 Retrieved from http://onlinelibrary.wiley.com/doi/10.1029/96JD01218/abstract

Khairoutdinov, M., & Kogan, Y. (2000). A new cloud physics parameterization in a large-eddy simulation model of marine stratocumulus. *Monthly Weather Review, 128*(1), 229-243. ANCPPI>2.0.CO;2 Retrieved from https://search.proquest.com/docview/198173215

Lacis, A. A. & Oinas, V. (1991) A description of the correlated-*k* distribution method for modelling nongray gaseous absorption, thermal emission, and multiple scattering in vertically inhomogeneous atmospheres. *Journal of Geophysical Research, 96*, 9027-9064.

Leaitch, W. R., Aliabadi, A. A., Willis, M. D., & Abbatt, J. P. D. (2016). Effects of 20-100 nm particles on liquid clouds in the clean summertime arctic. *Atmospheric Chemistry and Physics, 16*(17), 11107-11124. 10.5194/acp-16-11107-2016 Retrieved from http://search.proquest.com/docview/1824629793

Lenderink, G., & Holtslag, A. A. M. (2004). An updated length-scale formulation for turbulent mixing in clear and cloudy boundary layers. *Quarterly Journal of the Royal Meteorological Society*, 130, 3405–3427.

Li, J. (2002). Accounting for unresolved clouds in a 1D infrared radiative transfer model. Part I: Solution for radiative transfer, including cloud scattering and overlap. *Journal of the Atmospheric Sciences, 59*, 3302–3320.

Li, J., Curry, C. L., Sun, Z., & Zhang, F. (2010). Overlap of Solar and Infrared Spectra and the Shortwave Radiative Effect of Methane. *Journal of the Atmospheric Sciences, 67*, 2372-2389.

Li, J., Dobbie, S., Räisänen, P., & Min, Q. (2005). Accounting for unresolved clouds in a 1-D solar radiative-transfer model. *Quarterly Journal of the Royal Meteorological Society, 131*, 1607–1629.

Li, J., Scinocca, J., Lazare, M., McFarlane, N., von Salzen, K., & Solheim, L. (2006). Ocean surface albedo and its impact on radiation balance in climate models. *Journal of Climate, 19*(24), 6314-6333. 10.1175/JCLI3973.1 Retrieved from http://search.proquest.com/docview/222879266

Li, J., & Shibata, K. (2006). On the effective solar pathlength. *Journal of the Atmospheric Sciences, 63*, 1365–1373.

Liu, Y., & Daum, P. H. (2004). Parameterization of the autoconversion process.part I: Analytical formulation of the Kessler-type parameterizations. *Journal of the Atmospheric Sciences, 61*(13), 1539-1548. 10.1175/1520-0469(2004)061<1539:POTAPI>2.0.CO;2

Lohmann, U. (1996). Sensitivität des Modellklimas eines globalen Zirkulationsmodells der Atmosphäre gegenüber Änderungen der Wolkenmikrophysik. *Examensarbeit Nr. 41,* Max-Planck-Institut für Meteorologie, Hamburg, Germany.

Lohmann, U., & Roeckner, E. (1996). Design and performance of a new cloud microphysics scheme developed for the ECHAM general circulation model. *Climate Dynamics, 12*(8), 557-572. 10.1007/s003820050128

Mauritsen, T., Sedlar, J., Tjernstrom, M., Leck, C., Martin, M., Shupe, M., . . . Swietlicki, E. (2011). An arctic CCN-limited cloud-aerosol regime. *Atmospheric Chemistry and Physics, 11*(1), 165. Retrieved from http://lup.lub.lu.se/record/1876448

National Aeronautics and Space Administration. (2018). [Satellite data from EOSDIS Worldview on July 5, 7, and 8, 2014.] *NASA/Goddard Space Flight Center Earth Science Data and Information System (ESDIS) project*. Retrieved from https://worldview.earthdata.nasa.gov/

Olsson, P. Q., Harrington, J. Y., Feingold, G., Cotton, W. R., & Kreidenweis, S. M. (1998). Exploratory cloud-resolving simulations of boundary-layer arctic stratus clouds: Part I: Warm-season clouds. *Atmospheric Research, 47*, 573-597. 10.1016/S0169-8095(98)00066-0 Retrieved from https://www.sciencedirect.com/science/article/pii/S0169809598000660

Peng, Y., Lohmann, U., Leaitch, R., Banic, C., & Couture, M. (2002). The cloud albedo-cloud droplet effective radius relationship for clean and polluted clouds from RACE and FIRE.ACE. *Journal of Geophysical Research: Atmospheres, 107*(D11), 6. 10.1029/2000JD000281

Perovich, D. K., & Polashenski, C. (2012). Albedo evolution of seasonal arctic sea ice. *Geophysical Research Letters, 39*(8), n/a. 10.1029/2012GL051432

Pincus, R., Barker, H. W., & Morcrette, J.-J. (2003). A fast, flexible, approximate technique for computing radiative transfer in inhomogeneous cloud fields. *Journal of Geophysical Research*, *108*, 4376.

Sedlar, J., Tjernström, M., Mauritsen, T., Shupe, M., Brooks, I., Persson, P., . . . Nicolaus, M. (2010). A transitioning arctic surface energy budget: The impacts of solar zenith angle, surface albedo and cloud radiative forcing. *Climate Dynamics, 37*(7), 1643-1660. 10.1007/s00382-010-0937-5 Retrieved from http://search.proquest.com/docview/895305642

Shao, A., Qiu, C., Wang, X., & Zhang, Y. (2016). Using the newtonian relaxation technique in numerical sensitivity studies. *Science China Earth Sciences, 59*(12), 2454-2462. 10.1007/s11430-016-0033-3 Retrieved from https://search.proquest.com/docview/1848839151

Stevens, R. G., Loewe, K., Dearden, C., Dimitrelos, A., Possner, A., Eirund, G. K., . . ., Field, P. R. *A model intercomparison of CCN-limited tenuous clouds in the high arctic*10.5194/acp-2017-1128

Taylor, J., Edwards, J., Glew, M., Hignett, P., & Slingo, A. (1996). Studies with a flexible new radiation code. II: Comparisons with aircraft short-wave observations. *Quarterly Journal of the Royal Meteorological Society, 122*(532), 839-861. 10.1256/smsqj.53203

Terradellas, E., & Cano, D. (2007). Implementation of a single-column model for fog and low cloud forecasting at central-Spanish airports. *Pure and Applied Geophysics, 164*(6), 1327-1345. 10.1007/s00024-007-0221-8 Retrieved from https://doi.org/10.1007/s00024-007-0221-8

von Salzen, K., Scinocca, J. F., McFarlane, N. A., Li, J., Cole, J. N. S., Plummer, D., . . . Solheim, L. (2013). The Canadian fourth generation atmospheric global climate model (CanAM4). Part I: Representation of physical processes. *Atmosphere-Ocean, 51*(1), 104-125. 10.1080/07055900.2012.755610

Wood, R. (2005). Drizzle in stratiform boundary layer clouds. part II: Microphysical aspects. *Journal of the Atmospheric Sciences, 62*(9), 3034-3050. 10.1175/JAS3530.1 Retrieved from https://search.proquest.com/docview/236496166

Zdunkowski, W. G., Panhans, W.-G., Welch, R. M., & Korb, Gü. (1982). A Radiation Scheme for Circulation and Climate Models *Beiträge zur Atmosphärenphysik, 55*, 215-238.

Zhang, J., Lohmann, U., & Lin, B. (2002). A new statistically based autoconversion rate parameterization for use in large-scale models. *Journal of Geophysical Research: Atmospheres, 107*, 16. doi:10.1029/2001JD001484

Zhang, X., Musson-Genon, L., Dupont, E., Milliez, M., & Carissimo, B. (2014). On the influence of a simple microphysics parametrization on radiation fog modelling: A case study during ParisFog. *Boundary-Layer Meteorology, 151*(2), 293-315. 10.1007/s10546-013-9894-y Retrieved from http://search.proquest.com/docview/1509177985

APPENDIX A CALIBRATING THE FSSP-100 DROPLET DISTRIBUTION

Description of how to calibrate the FSSP-100 droplet distribution based on emails from Richard Leaitch.

From the FSSP, we need:

- the mid-point diameter of each size bin
- number of droplets counted per second
- sum of the number of droplets counted per second
- number concentrations calculated by software in the data acquisition system during flight using the counts per second
- LWCs per bin, based on the original FSSP number concentrations
- sum of the original LWCs per bin
- volume-weighted mean diameter based on r^3=(LWC/[N*4*pi/3])
- valid counts

We also need the true air speed of the aircraft, which in this case came from the AIMMS-20 measurements.

The theoretical factor of the FSSP (0.62) is based on geometric considerations of the transit time of a particle through the sample volume of the FSSP (Leaitch et al., 2016). The depth of field of the laser beam was measured in a lab and in-situ on the ground (Leaitch, personal communication). The beam diameter is the diameter of the laser beam produced by the FSSP to measure the droplet counts and sizes. The depth of field, beam

diameter, and theoretical factor are assumed to be constant (Leaitch, personal communication).

Correcting formulas:

calibrated total number concentration = [valid counts] / ([measured depth of field] * [measured beam diameter] * [theoretical factor] *[true air speed (m/s)])

calibrated total number concentration at STP = (1013.12)/[pressure in hPa] * [calibrated total number concentration] * ([temperature in K] / temperature at STP)

calibrated LWC = [calibrated total number concentration at STP] / [original total concentration] * [original LWC]

To calculate droplet size parameters, use number concentrations per bin with sizes when only relative number concentrations are needed.

Note: This does not include corrections for coincident droplets or probe dead-time.

APPENDIX B CONTRIBUTIONS

Joelle Dionne: fixed the FSSP-100 total LWC and droplet distribution data, compiled input files for the SCM-ABLC, ran the SCM-ABLC, examined satellite imagery to estimate albedo values, compiled input files for the cloud variables and albedo for the radiative transfer model, ran the radiative transfer model, examined and plotted SCM-ABLC output, examined and plotted radiative transfer model output, wrote this document.

Rachel Chang: project direction, edited this document.

Jason Cole: provided the radiative transfer model and a lot of advice on how to run it.

Ian Folkins: provided useful insight on issues with the SCM-ABLC and what we were doing with it, project direction.

Richard Leaitch: background on the NETCARE 2014 campaign data collection, explained how to fix the FSSP-100 total LWC and droplet distribution, provided observational data.

Glen Lesins: useful insight on how to best start investigating with the radiative transfer model.

Rashed Mahmood: compiled all of the input files for the radiative transfer model except for cloud variables and albedo.

Knut von Salzen: provided the SCM-ABLC, a lot of advice on how to make input files and run it, project direction.